An Indicative Model Considering Part of the Thermo-Mechanical Behaviour of a Large Grinding Machine

Martin Mareš[1]([✉]), Otakar Horejš[1], and Pravoslav Nykodym[2]

[1] Faculty of Mechanical Engineering, Department of Production Machines and Equipment, RCMT, Czech Technical University in Prague, Horská 3, 128 00 Prague, Czech Republic
m.mares@rcmt.cvut.cz
[2] TOS Hostivař s.r.o., Rádiová 1431/2a, 102 00 Praha 10, Czech Republic

Abstract. Machine tool (MT) thermal errors are an important element in machined workpiece inaccuracies. In the past few decades, thermal errors associated mainly with one particular source (e.g. spindle or environment), have been successfully reduced by SW compensation techniques such as multiple linear regression analysis, finite element method, neural network, transfer function (TF) within similar calibration and verification conditions. An approach based on TFs is used for thermal error modelling in this research. This method respects basic heat transfer mechanisms in the MT and requires a minimum of additional gauges. The approach provides insight into the share of each source in the total machine thermal error through a combination of linear parametric models. The aim of this research is to develop an indicative model for a large grinding machine with predictive functionality focused on part of the thermo-mechanical behaviour within different configurations of the headstock, tailstock and workpiece. Unlike a compensation model, an indicative model has no connection to the MT feed drives and can only provide the machine operator with information regarding the actual direction and relative magnitude along with prediction of the time constant and steady state of the non-stationary thermal error. The second aim is to compare the difficulty of measuring at the stator and rotating machine part levels, the thermal behaviour linearity at both levels and the possibility of upgrading the indicative model to a compensation model to extend industrial applicability.

Keywords: Grinding Machine · Thermal Errors · Control Limits

1 Introduction

The heat generated e.g. by moving axes and machining processes creates thermal gradients, resulting in the thermal elongation and bending of machine tool (MT) elements, which substantially deteriorate MT accuracy. Consequently, up to 75% of all geometrical errors of machined workpieces are caused by temperature effects [1]. Thermal errors may be sufficiently reduced by new MT design concepts which are less sensitive to thermal effects. This type of intervention in the MT structure leads to a pareto set of different

parameters, and designers have to concentrate on preserving other MT properties as well [2]. Redesigning the MT structure is usually possible in the prototype phase of new products. Adaptive or intelligent control of cooling systems [3], integrated additional sensors in the MT structure [4] or direct (in-process) measurement techniques [5] may also be very efficient in minimising thermo-mechanical impacts on MT accuracy. However, they do increase machine and operational costs and result in machining process interruptions and prolonged production time. A very promising contemporary approach is the use of finite element method (FEM) [6], especially coupled with model order reduction (MOR) techniques to reduce computing time [7]. The problem of boundary condition complexity at the machine or component level, however, is still present in this solution. In contrast, indirect (software) compensation of thermal errors at the tool centre point (TCP) is one of the most widely employed reduction techniques due to its cost-effectiveness and ease of application. Different types of software error compensation are becoming a crucial part of modern technological development in the context of Industry 4.0 and intelligent MT [8].

Ordinarily, approximation models are based on measured auxiliary variables [9] (temperature, spindle speed, etc.) used to calculate the resulting thermally induced displacements at the TCP. Many strategies have been investigated to establish these models, e.g. multiple linear regressions (MLR) [10], artificial neural networks (ANN) [11], transfer functions (TF) [9], etc. The majority of the compensation models introduced in the literature have the potential to significantly reduce MT thermal errors. The methods differ in the amount and type of input variables, and the training and modelling time required for composition and model architecture (white, black or grey-boxes [12]). Therefore, efforts should be focused on the applicability and verification of approaches in real industrial conditions to meet end-users' needs as well.

An approach to thermal error modelling of a large turning-milling centre in regard to various MT configurations was presented in [13], followed by a presentation of the limits of a similar linear parametric model in compensating efforts for the effect of different grinding wheels on the thermal behaviour of a large grinding machine [14]. In this research, the approach is further advanced and critically evaluated by application on the same large grinding machine but within the headstock and tailstock activity with varying axial and radial force. The implementation and application possibilities of the designed thermal error models on the stator and rotor MT part levels are discussed here.

The rest of the paper is arranged as follows: in Sect. 2, the experimental setups and conditions are described. In Sect. 3, the measured data and analysis are presented. The modelling approach is described in Sect. 3.3 in more detail along with an indicative model structure applied on the measured data. Based on the results the model is upgraded to compensate for thermal errors. All of the results are critically discussed in Sect. 4, followed by conclusions and the outlook for further research.

2 Experimental Setup and Conditions

The target machine for this article is a large grinding machine for round grinding operations. The machine consists of two separate beds. The front bed carries a headstock and a tailstock movable along the Z-axis. The linear movement of both components serves

for positioning the workpiece. The workpiece clamped in the headstock performs a rotational movement. The rear bed carries a wheel head movable in the X and Z directions as shown in Fig. 1. The maximum diameter of the grinding wheel is 915 mm with rotation of 1350 rpm. The maximum diameter of a clamped workpiece is 1000 mm, the length is 4000 mm and the weight is 9000 kg. The maximum speed of a headstock spindle is 50 rpm and the axial force exerted by the tailstock for workpiece clamping is 60 kN. The machine bodies are made of cast iron.
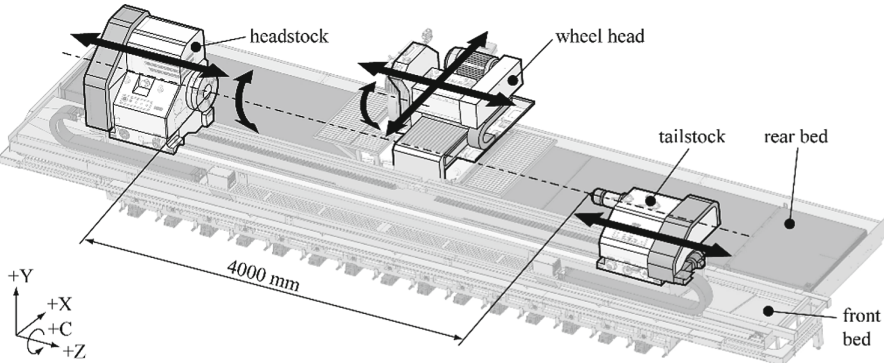

Fig. 1. Schema of the target machine with the indicated kinematics.

The target machine was placed in a MT manufacturer's assembly room. The room is a huge, unair-conditioned open space equipped with a row of production machines. Despite the character of the room, the environment is considered stable during the tests.

Basically, grinding machines for round grinding are capable of simultaneous rotation realised in three components: the wheel head (rotation of the grinding wheel), headstock and tailstock (rotation of the workpiece). This research is focused on the impact of workpiece rotation on MT thermal error. The MT is considered in three configurations. The schema of the machine in a configuration with the workpiece clamped with the 'loose end' in chuck is depicted on the left side of Fig. 2. The workpiece is represented by the testing mandrel. The schema of the machine in a configuration with a small workpiece clamped 'between the centres' of the headstock and tailstock is depicted on the right side of Fig. 2. The tailstock exerts a clamping force on the workpiece, causing an axial load on the headstock and tailstock bearings. The schemas contain the approximate positions of three temperature probes (Pt100, Class A, 3850 ppm/K; headstock bearings temperature $T_{\text{hs bearings}}$, tailstock bearings temperature $T_{\text{ts bearings}}$ and reference temperature $T_{\text{reference}}$ reflecting changes in the environment). These sensors are embedded in the MT control system. The schema of the machine in the third configuration with a large workpiece (1800 kg) clamped 'between the centres' is depicted on the left side of Fig. 3. The weight of the workpiece adds a radial load on the bearings. The location of the deformation sensors on the machine in the third configuration is indicated on the right side of the same figure. Displacements were measured between the stator parts of both components ($\delta_{\text{X stat}}$; indicating relative displacement of the entire headstock and wheel head bodies) and between their axes of rotation ($\delta_{\text{X rot}}$; displacement reflecting the direct impact on

workpiece accuracy, mostly subject to compensation). Eddy-current sensors (PR6423) clasped in magnetic holders were used for noncontact sensing of displacements between the rotating parts and contact probes (Peter Hirt T100) between the stators.
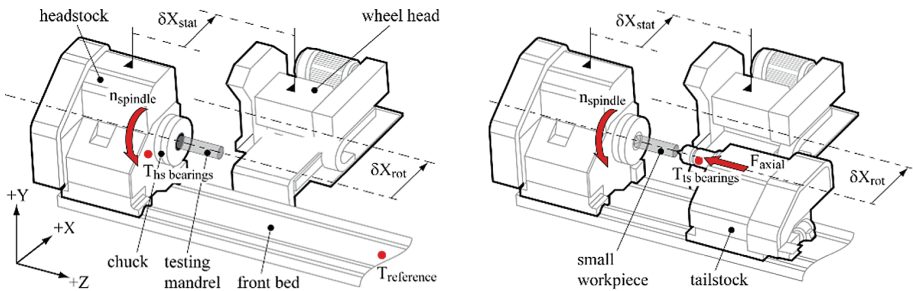
Fig. 2. Schema of the experimental setup with headstock activity during rotation of the clamped testing mandrel (left) and with clamped small workpiece (right).
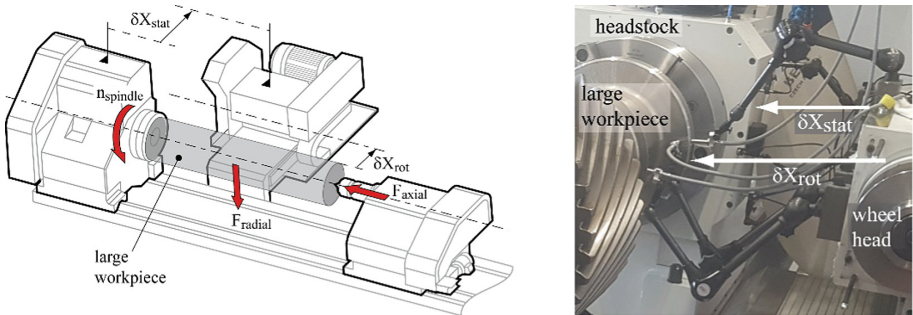

Fig. 3. Experimental setup with headstock and tailstock activity with clamped large workpiece: schema (left), on machine (right).

Four experiments were carried out within the three machine configurations. The experimental setups are summarised in Table 1.

Detailed setup and conditions of the realised tests are shown in Fig. 4, containing the headstock spindle speed and axial and radial forces applied over 4 days of testing. The highlighted area of the test 2 heating phase is intended for calibration of the models. Each test consists of a part of the transient behaviour between two thermodynamic equilibria (the MT in approximate balance with its surroundings and the MT steady state during heat source activity), concluded after one work shift (6 to 8 h) followed by a cooling phase (16 to 18 h). Test 3 extends tests 1 and 2 with the addition of axial force and test 4 extends the settings with the addition of radial force application. The rpm settings of test 1 and test 2 differ. The four tests are designed to evaluate the linearity of MT thermo-mechanical behaviour. Process cooling and the process itself were inactive during testing. The positions of the headstock and wheel head were similar in all of the setups. Further efforts are focused on the main direction X of the machine generally affecting the accuracy of the ground workpiece diameter.

Table 1. Setup of realised tests.

Test no.	Machine configurations	Active heat source	Rotation speed [rpm]	Axial force [kN]	Radial force [kN]
1	loose end (testing mandrel)	Headstock	35	–	–
2	loose end (testing mandrel)		50		
3	between the centres (small workpiece)	Headstock and tailstock	50	60	
4	between the centres (large workpiece)		35	30	18
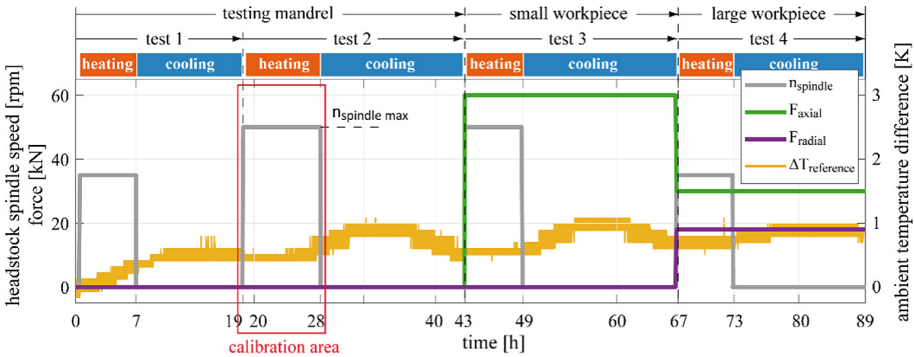
Fig. 4. Spindle speed, axial and radial force profiles along with ambient temperature changes during tests 1 and 2 (testing mandrel), 3 (light workpiece) and 4 (large workpiece).

3 Thermal Error Analyses, Model Developments and Verification

3.1 Modeling Approach and Efficiency Evaluation Method

The concept behind the modelling approach lies in the usage of a minimum of additional gauges (only from the MT control system [9]), an open structure that is easy to extend and modify (advantageous for machine learning principles [16]), real time application and ease of implementation into MT control systems.

A compensation strategy based on TFs is a dynamic method with a physical basis. A discrete TF is used to describe the link between the excitation and its response:

$$y(t) = u(t) \cdot \varepsilon + e(t) \tag{1}$$

The vector $\boldsymbol{u}(t)$ in Eq. (1) is the TF input and $\boldsymbol{y}(t)$ is the output vector in the time domain, ε represents the general TF in the time domain, and $\boldsymbol{e}(t)$ is the disturbance value (further neglected). The TF form of polynomials' quotient is expressed by Eq. (2).

$$\frac{Z\{y(t)\}}{Z\{u(t)\}} = \frac{a_n \cdot z^{-n} + \cdots + a_1 \cdot z^{-1} + a_0 \cdot z^0}{b_m \cdot z^{-m} + \cdots + b_2 \cdot z^{-2} + b_1 \cdot z^{-1} + b_0 \cdot z^0}, \tag{2}$$

where Z is the Z-transform of the time discretized function, z is the complex variable, n is the order of the TF numerator, m is the order of the TF denominator and holds that $m > n$. Further, $a_{0:n}$ are the calibration coefficient of the TF input, and $b_{0:m}$ are the calibration coefficient of the TF output. The difference form of the discrete TF (a generally suitable form for modern MT control systems using their programming languages) in the time domain is introduced in Eq. (3).

$$y(k) = \frac{u(k-n) \cdot a_n + \cdots + u(k-1) \cdot a_1 + u(k) \cdot a_0 - y(k-m) \cdot b_m - \cdots - y(k-1) \cdot b_1}{b_0}, \tag{3}$$

where k represents the examined time instant and $k - n$ $(k - m)$ is the n-multiple (m-multiple) delay in the sampling frequency 1 s^{-1} of the measured input vector (simulated output vector). A linear parametric model with an autoregressive with external input (ARX) identifying structure is used with the help of *Matlab Identification Toolbox* [15]. The ARX as an optimal model structure (with the best fit in quality and robustness) is also discussed in [16].

The approximation quality of the simulated behaviour is expressed by a global approach based on the least square method (*fit*; a percentage value where 100% would equal a perfect match of the measured and simulated behaviours):

$$fit = \left(1 - \frac{\|\boldsymbol{measured} - \boldsymbol{simulated}\|}{\|\boldsymbol{measured} - mean(\boldsymbol{measured})\|} \right) \cdot 100. \tag{4}$$

The **measured** value in Eq. (4) is the measured output (here displacements in the X direction), **simulated** is the simulated model output, and *mean*(**measured**) expresses the arithmetic mean of the measured output over time.

3.2   Linearity Analyses of Thermo-Mechanical Behaviour

An analysis of the linearity between the input (measured temperature) and the outputs (measured deformations) of the thermal mechanical system during the heating phases of the 4 tests at the level of the stators and the axis of rotation is shown in Fig. 5.

The results demonstrate that changing the experimental setup does not affect the linearity of the whole system at the level of the stator parts of the components (due to its informative nature only, the expression is in relative values, however, the axis division of the two diagrams is equally selected) in contrast to the level of the rotation axes, where the change in the test settings affects the gain of thermo-mechanical transient behaviour while maintaining similar time constants. Thus, the modelling difficulty at the two levels differs considerably. This also confirms the assumption of a higher system linearity on the shorter links of the machine's kinematic chain.
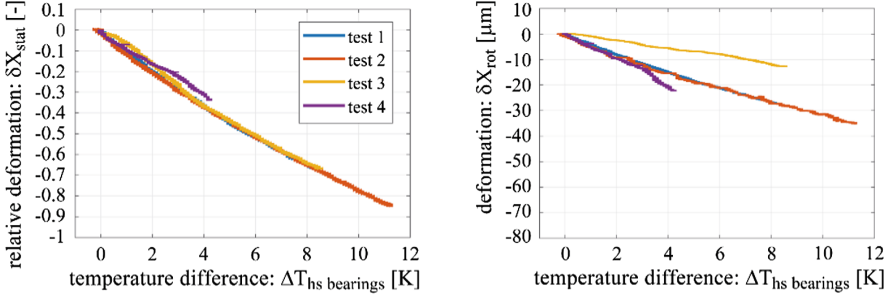
Fig. 5. Linearity analysis between the temperature of the headstock bearings and the deformations measured on the stators (left) and axes of rotation (right) during the heating phases of the tests.

3.3 Indicative Model of MT Thermal Behaviour with Predictive Functionality

Working on grinding machines generally requires high precision and reliability. Both producers and users are reluctant to fully rely on any built-in indirect compensation approaches in control systems. Frequent measurement of the workpiece geometric accuracy and considerable operator experience are required. The following section presents the functionality of the thermal error model within the expert system with predictive functions, providing the operator with informative data for better orientation, expectation and understanding of the machine's behaviour during the current process.

The expected functionalities of the expert system are as follows:

A) Determination of the development and direction of the thermal error in accordance with the machine coordinate system;
B) estimation of the time constants of transient phenomena;
C) prediction of the time to reach a steady state during the activity of the described heat source, assuming that the power value of the source would not change.

This is possible based on a known power input quantity to the model. In this case, the input is the course of headstock spindle revolutions. The model for estimating the behaviour of headstock spindle bearings' temperature change is given in Eq. (5).

$$\Delta T_{hs\,bearings}^{simulated} = \boldsymbol{n}_{spindle} \cdot \gamma_{test\,2} \cdot k_{\vartheta},\tag{5}$$

where $\Delta T_{hs\,bearings}^{simulated}$ is the simulated vector of the temperature difference, $\gamma_{test\,2}$ is the identified 2nd order discrete TF in the time domain with power excitation (calibration coefficients are summarised at the end of the section) and k_{ϑ} is the correction factor between the simulated and measured temperature unique for each test. Given the measured temperature values that are available, it is possible at any time t_j to adapt the simulated value to the measured reality according to Eq. (6).

$$k_{\vartheta} = \frac{\Delta T_{hs\,bearings}^{measured}\left(t_j\right)}{\Delta T_{hs\,bearings}^{simulated}\left(t_j\right)}\tag{6}$$

The model input during calibration test 2 and the measured and simulated behaviours of the temperature changes during the heating phases of all tests are depicted in Fig. 6.
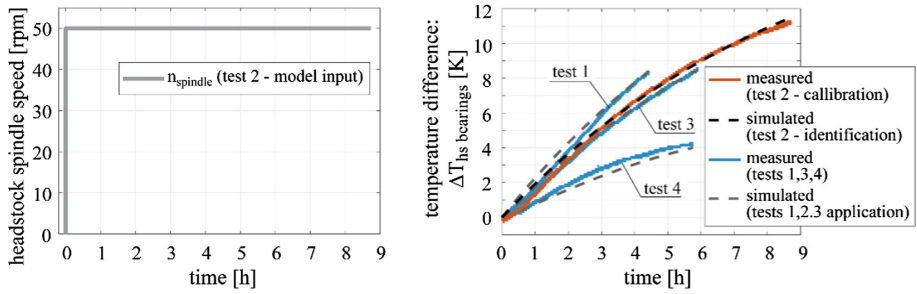
Fig. 6. Model input vector of the recorded headstock spindle speed during the heating phase of calibration test 2 (left) and the headstock bearing temperatures, measured and simulated according to Eq. (5) during the heating phases of all tests 1 to 4 (right).

Generally, indicative models have no link to the MT feed drives and can only provide the machine operator with data of an informational nature. The description of the indicative model of the temperature errors caused by the rotation of the workpiece, respecting the different settings of all tests, benefiting from the linear behavior of the deformations at the level of the stator parts of the components (see the left side of Fig. 5), and the predictive properties of the model from Eq. (5), follows in Eq. (7).

$$\delta X_{stat}^{simulated} = \left(n_{spindle} \cdot \gamma_{test\,2} \cdot k_{\vartheta} \right) \cdot \varepsilon_{test\,2}, \qquad (7)$$

where $\delta X_{stat}^{simulated}$ is the simulated vector of relative deformations at the stator parts of the MT components, $\varepsilon_{test\,2}$ is the identified 3rd order discrete TF in the time domain with temperature excitation (calibration coefficients are summarised at the end of the section). The results of identification (test 2) and application (test 1, 3 and 4) of the indicative model for the heating phases are shown on the left side of Fig. 7. Predictive functionality, assuming the same technological parameters of the current process, estimating the time to reach the steady state and calculating the time constant τ of the transition phenomenon, is shown on the right side of Fig. 7 for the test 4.
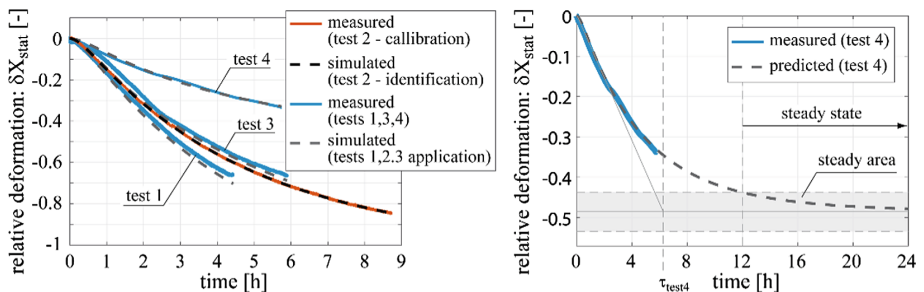
Fig. 7. Relative deformations, measured and simulated by the indicative model (Eq. (7)), on the stators of the headstock and wheel head during heating phases of all tests 1 to 4 (left) and demonstration of the model's predictive functionality during the heating phase of test 4 (right).

The figure shows that in the case of the test 4 setup, a stable area (10% envelope of the steady state point) will be reached after 12 h of heat source activity. The calculated time constant of the transient phenomenon from the predicted behaviour of test 4 is $\tau_{\text{test}4} = 6.5$ h. This information, data and the trends contained in the expert system can be provided to the operator both in terms of temperatures (Eq. (5)) and deformations (Eq. (7)) to help plan production progress on the machine.

3.4   Upgrade of Indicative Model to Compensate for Thermal Errors

The right side of Fig. 5 shows obvious differences in the linear dependence between the temperature near the heat source and the deformations measured at the axes of the rotation level. The model from Eq. (7) may be updated to the compensation level of Eq. (8) by finding the transfer between the deformations of the stator parts and the deformations at the rotation level axes and including a simple gain-scheduling problem [17] in the model structure.

$$\delta X_{rot}^{simulated} = \left[\left(\boldsymbol{n}_{spindle} \cdot \gamma_{test\,2} \cdot k_{\vartheta} \right) \cdot \varepsilon_{test\,2} \right] \cdot \delta_{test\,2} \cdot k_{test\,i}, \tag{8}$$

where i indicates the tests 1, 2, 3, 4. The $\delta X_{rot}^{simulated}$ in Eq. (8) is the simulated vector of deformations at the rotation level axes, $\delta_{test\,2}$ is the identified 1st order discrete TF in the time domain with deformational excitation (calibration coefficients are summarised at the end of the section) and $k_{test\,i}$ is the adaptive gain factor depending on time $t_{test\,i}$ and measured deformation and is unique to each machine configuration. Time $t_{test\,i}$ is determined for each test setting when the value of the adaptation factor according to Eq. (9) stabilizes and does not change any further.

$$k_{test\,i} = \frac{\delta \boldsymbol{X}_{rot}^{measured}(t_{test\,i})}{\delta \boldsymbol{X}_{rot}^{simulated}\left(k_{test\,1,2}, t_{test\,i} \right)}, \text{ where } k_{test\,1,2} = 1 \text{(model calibration).} \tag{9}$$

The results of the compensation model from Eq. (8) application along with the high-lighted values of the adaptation coefficients and the time required for their determination are shown on the left side of Fig. 8. The right side contains the theoretical values of the residual thermal errors after compensation model application.

The application of the model from Eq. (8) to test 4 (3.7 µm) shows the largest residual error, the smallest to test 1 (1.3 µm). The total residual deformation over all tests reaches a value of 4.5 µm. The determined uncertainty of deformation measurement is ±0.92 µm.

The following table lists all the calibration coefficients of the identified TFs in Eqs. (5), (7) and (8) and the maximum approximation quality achieved during the iden-tification process. The achieved approximation quality is one of the criteria for choosing a TF in the model structure. The second criterion is the TF stability check verified by linear time invariant (LTI) step response [15]. LTI expresses a clear dependency between an input (unit jump of TF excitation) and output (predicted TF response) of the thermo-mechanical system. LTI diagrams with the TF responses to unit excitations are shown in Fig. 9. The graphs enable a better understanding of the links in the investigated thermo-mechanical system.
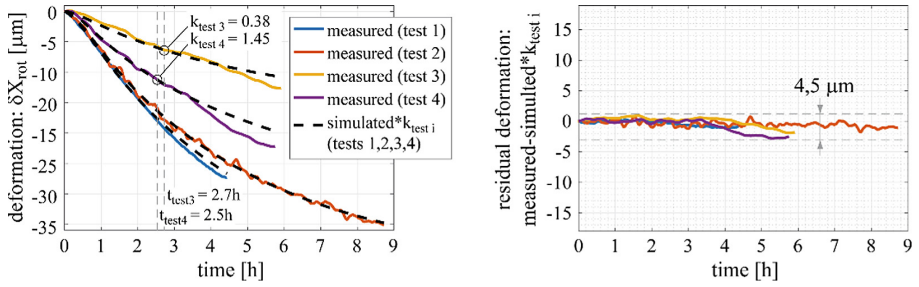
Fig. 8. Deformations on rotation level axes of the headstock and wheel head during heating phases of all tests 1 to 4, measured and simulated by compensation model (Eq. (8)) (left) and demonstration of residual errors after the model application (right).

Table 2. Identified parameters of thermal error model.

TF	a_0	a_1	b_0	b_1	b_2	b_3	fit
$\gamma_{test\ 2}$	$7.3665e-07$	0	1	-1.93457	0.93457	0	92%
$\varepsilon_{test\ 2}$	-0.16306	0.16305	1	-0.71385	0.10325	-0.38936	95%
$\delta_{test\ 2}$	0.1063	0	1	-0.9975	0	0	94%
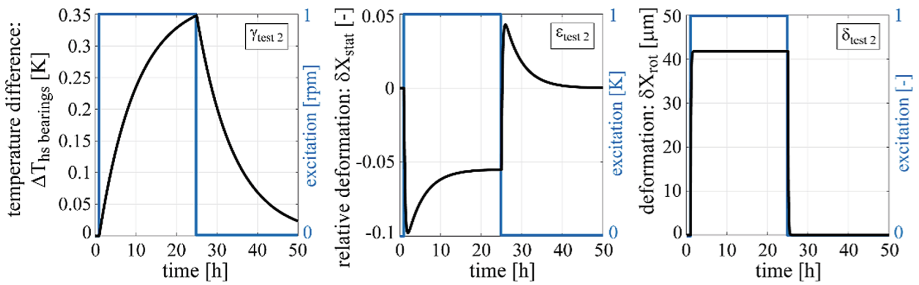
Fig. 9. LTI step responses of identified TFs in the compensation model (Eq. (8)) to headstock spindle speed (left), temperature difference of headstock spindle bearing (middle) and relative deformations on machine stator parts (left) unit excitation.

4   Discussion of Results and Conclusions

The axial and radial bearings load has no observable influence on the linearity of the thermo-mechanical behaviour (as can be seen from the dependence of temperatures and deformations on the level of the stators of the target machine; see right side of Fig. 5). The system is retuned by changing the clamping of the workpiece from 'loose end' to 'between the centres', manifested by a change in the linear dependence of temperatures and deformations at the rotation level axes. This fact is caused by another heat source engaged in the kinematic chain of the machine - the tailstock. The inclusion of the

tailstock results in a significant angular error of the Z-axis of the workpiece in the *xz* plane, thus emphasising the influence of clamped workpiece dimensions.

An accurate grinding process requires frequent in-process measurement of the ground surface accuracy. The indicative model (Eq. (7)) helps the operator when the measurement needs to be intensified, otherwise, when frequent measurement is redundant due to the thermal stability of the machine. The indicative model has been implemented into the control system of the machine as interactive diagnostic screens via a superstructure environment by mySCADA technology programmed in Javascript.

The compensation model (Eq. (8)) finds practical applications in the machining of long workpieces, which requires a long time for one operation without interruption by measuring the geometric accuracy of the workpiece. The effectiveness of the compensation model applied to a complete, uninterrupted experiment from Fig. 4 is demonstrated in Fig. 10. The approximation quality drops from an average of 87% to 63% compared to heating phase only compensation, as can be seen from the last row in Table 3. The residual deformation more than doubles, from 4.5 µm to 10.5 µm. The model shows good long-term stability due to the small influence of the surrounding environment. The approximation of the entire progress may be refined by including the cooling phase in the calibration measurement. However, this approach will either negatively affect the approximation of the heating phase or complicate the structure of the model with another TF describing the cooling phase with the requirement to control the switching between approximations of both phases.
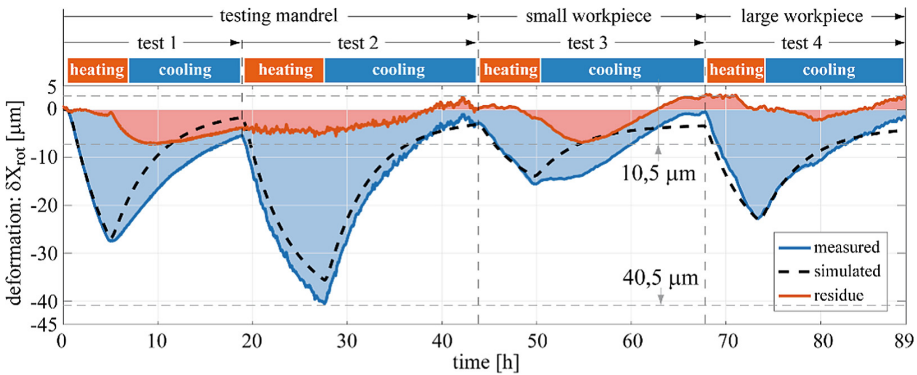
Fig. 10. Results of compensation model (Eq. (8)) application on the entire measurement.

A critical evaluation of the presented models follows. The indicative model does not need any correction factors. Its outputs are only informative (with predictive functionalities) and are expressed in relative values. The achieved average efficiency of the indicative model is 93% within this research. The informative indicative model can be upgraded to the compensation model with an action link to the machine's feed drives. The compensation model requires adaptive gain-scheduling elements obtained from direct measurements and its average efficiency is 5% lower (88%). The compensation has a direct positive link to the increase in the geometric accuracy of the workpiece and is

Table 3. Approximation quality of indicative and compensation models.

Test No.	1	2 (calibration)	3	4	Whole behaviour
Model	*fit*				
Indicative (Eq. (7))	91%	95%	91%	93%	–
Compensation (Eq. (8))	93%	94%	81%	81%	63%

carried out in the background of the process without the necessary intervention (or even awareness) of the operator.

Measuring the mutual displacement of the stator parts of the machine to further extend the validity of the indicative model is easier to implement, especially by using laser interferometry. Contrarily, it is convenient, but more difficult, to obtain data for the compensation model directly from accuracy measurements on the workpiece.

Future research will focus on the positional dependence of machine thermal errors, the influence of process fluid in the concept of an energy-efficient machine, hybrid compensation (using both direct and indirect compensation strategies) and extending the model applicability depending on the FEM outputs.

References

1. Mayr, J., et al.: Thermal issues in machine tools. CIRP Ann. – Manuf. Technol. **61**(2), 771–791 (2012)
2. Grossmann, K.: Thermo-Energetic Design of Machine Tools: A Systemic Approach to Solve the Conflict Between Power Efficiency, Accuracy and Productivity Demonstrated at the Example of Machining Production. Lecture Notes in Production Engineering, p. 260. Springer, Cham (2015). https://doi.org/10.1007/978-3-319-12625-8. ISBN 978-3-319-12624-1
3. Hellmich, A., Glänzel, J., Ihlenfeldt, S.: Methods for analyzing and optimizing the fluidic tempering of machine tool beds of high performance concrete. In: CIRP-Sponsored 1st Conference on Thermal Issues in Machine Tools, Dresden, Germany (2018)
4. Naumann, C., Brecher, C., Baum, C., Tzanetos, F., Ihlenfeldt, S., Putz, M.: Hybrid correction of thermal errors using temperature and deformation sensors. In: CIRP-Sponsored 1st Conference on Thermal Issues in Machine Tools, Dresden, Germany (2018)
5. Zimmermann, N., Mayr, J., Wegener, K.: Extended discrete R-test as on-machine measurement cycle to separate the thermal errors in Z-direction. In: Proceedings of the Euspen's Special Interest Group: Thermal Issues, Aachen, Germany, pp. 21–24 (2020)
6. Glänzel, J., Naumann, A., Kumart, T.S.: Parallel computing in automation of decoupled fluid-thermostructural simulation approach. J. Mach. Eng. **20**(2), 39–52 (2020)
7. Hernández-Becerro, P., Spescha, D., Wegener, K.: Model order reduction of thermal models of machine tools with varying boundary conditions. In: CIRP-Sponsored 1st Conference on Thermal Issues in Machine Tools, Dresden, Germany (2018)

8. Liu, K., Liu, H., Li, T., Liu, Y., Wang, Y.: Intelligentization of machine tools: comprehensive thermal error compensation of machine-workpiece system. Int. J. Adv. Manuf. Technol. **102**(9–12), 3865–3877 (2019). https://doi.org/10.1007/s00170-019-03495-7
9. Brecher, C., Hirsch, P.: Compensation of thermo-elastic machine tool deformation based on control internal data. CIRP Ann. – Manuf. Tech. **53**(1), 299–304 (2004)
10. Naumann, C., Glänzel, J., Putz, M.: Comparison of basis functions for thermal error compensation based on regression analysis – a simulation based case study. J. Mach. Eng. **20**(4), 28–40 (2020)
11. Mize, C.D., Ziegert, J.C.: Neural network thermal error compensation of a machining center. Prec. Eng. **24**(4), 338–346 (2000)
12. Li, J.W., Zhang, W.J., Yang, G.S., Tu, S.D., Chen, X.B.: Thermal-error modeling for complex physical systems: the-state-of-arts review. Int. J. Adv. Manuf. Technol. **42**, 168–179 (2008)
13. Mareš, M., Horejš, O., Hornych, J.: Thermal error minimization of a turning-milling center with respect to its multi-functionality. Int. J. Autom. Technol. **14**(3), 475–483 (2020)
14. Horejš, O., Mareš, M.: Limits of linear parametric models for thermal error compensation of a large grinding machine. In: Proceedings of the Euspen's Special Interest Group: Thermal Issues, 4 p. ETH, Zurich (2022)
15. Ljung, L.: System identification toolbox™ user's guide. The MathWorks (2015)
16. Blaser, P., Mayr, J., Wegener, K.: Long-term thermal compensation of 5-axis machine tools due to thermal adaptive learning control. MM Sci. J. **4**, 3164–3171 (2019)
17. Rugh, W.J., Shamma, J.S.: Research on gain scheduling. Automatica **36**(10), 1401–1425 (2000)